JOURNAL OF SOLID STATE CHEMISTRY 69, 153–161 (1987)

X-Ray Absorption Study of the ZrO_2–Y_2O_3 System

M. H. TUILIER, J. DEXPERT-GHYS,* H. DEXPERT, AND P. LAGARDE

*LURE, Laboratoire CNRS-CEA-MEN, Bâtiment 209D, Université de Paris-Sud, 91405 Orsay Cédex, and *Laboratoire des Elements de Transition dans les Solides, CNRS, 1 Place A. Briand, 92195 Meudon Cédex, France*

Received July 10, 1986

A complete EXAFS analysis of the ZrO_2–Y_2O_3 system has been performed at both the yttrium and zirconium K absorption edges. The main result of this work is that the first average cation–oxygen distances are quite different and remain similar to those known for the pure oxides, namely, 2.16 Å for ZrO_2 and 2.28 Å for Y_2O_3. The EXAFS spectra show qualitatively that the yttrium network is much more sensitive to the Y^{3+}/Zr^{4+} substitution than the zirconium one.

I. Introduction

The zirconium-rich side of the ZrO_2–Y_2O_3 system is well known as yttria-stabilized zirconia (YSZ) phases. These play a major role in the ceramic industry. Although a considerable amount of work on the mechanical and electrical characteristics of YSZ has been published, relatively little deals with the microscopic structure of these compounds.

The EXAFS spectroscopy is a technique particularly well suited to investigate such phases were a large amount of structural disorder exists. We report here the detailed EXAFS analysis at the yttrium and zirconium K edges of several compositions in the ZrO_2–Y_2O_3 system. Preliminary results have been given already (*1*) and were consistent with a simultaneous study by Goldman *et al.* (*2*) on a more restricted part of the ZrO_2–Y_2O_3 phase diagram.

The YSZ-type phases exhibit a cubic fluorite-type structure over a large range of composition. The substitution of M^{4+} by M'^{3+} starting from an ideal MO_2 phase creates oxygen vacancies which are responsible for the anionic conductivity at elevated temperature (*3*). The fluorite-type YSZ are usually described by a statistical distribution of Zr^{4+} and Y^{3+} ions in the cationic lattice together with a random distribution of oxygen vacancies in the anionic sublattice. On the other hand, the cubic Y_2O_3 structure is deduced from the fluorite one with a double unit cell in which oxygen vacancies are ordered along [111] axes. The Y^{3+} point symmetry is either C_2 (three-fourths of the ions) or S_6 (one-fourth of the ions). Pure ZrO_2 exhibits a distorted fluorite monoclinic structure at room temperature. One of us (*4*) used the partial substitution of Y^{3+} by Eu^{3+} acting as an optical structural microprobe to get information about the position and the local ordering of vacancies with respect to the cations. The main

0022-4596/87 $3.00

results of that previous work, performed on 18 compositions in the $Zr_{1-x}(Y, Eu)_xO_{2-0.5x}$ system, were the following:

—The stabilization process which was observed for $x \geqq 0.04$ was accompanied by a drastic change in the immediate surroundings of the cations by comparison with nonstabilized zirconia. On the other hand, a continuous evolution of the Eu^{3+} fluorescence spectrum was observed for the different stabilized forms: tetragonal ($0.04 \leqq x \leqq 0.10$), cubic fluorite (F) ($0.18 \leqq x \leqq 0.82$), and cubic C–Ln_2O_3 ($0.67 \leqq x \leqq 1$).

—A structural model was built in which cations are surrounded by 8, 7, and 6 oxygen atoms as first neighbors with increasing x.

—The major indication given by the local probe was that the anionic sublattice accommodates randomly located vacancies, which causes complex oxygen displacements, giving rise to what may be described as a glass of anions. That was clearly evidenced by the low Eu^{3+} symmetries and the large fluorescence linewidths observed. The shortcomings of that optical microprobe analysis are the impossibility of evaluating the average Eu^{3+} environment and the indetermination inherent to the partial substitution by the active ions. In fact, because of their similar chemical properties, Eu^{3+} was thought to substitute for Y^{3+} but the extent to which this substitution does distort the actual yttrium site is not known.

II. Materials, Data Acquisition, and Analysis

Samples were obtained by coprecipitation of the corresponding hydroxides and drying and firing in a lime-stabilized heating element at 1750–1800°C over about 20 hr. Experimental details were given in (*4*). The samples analyzed by EXAFS were those synthesized for the optical measurements and therefore contain a very low amount of europium (0.5 to 1 atomic percent of the whole cationic content). The effect of europium, if any, has not been considered in the present study.

The samples were first analyzed by X-ray diffraction as reported in Table I. Three structural modifications are observed in yttria-stabilized zirconias: tetragonal (sample E), cubic fluorite (samples D and C), and cubic C–Ln_2O_3 type (sample B). The earlier reported $Zr_3Y_4O_{12}$ ordered phase (*5*, *6*) has never been observed in our samples either by X-ray or by electron diffraction (*7*).

The X-ray absorption data of these powdered samples have been recorded at room temperature at the yttrium and zirconium K edges using synchrotron radiation emitted by the DCI storage ring operating at 1.85 GeV. The monochromator was a Si (311) double crystal allowing harmonic rejection.

The EXAFS spectra have been analyzed using a now well-known procedure. The pre-edge absorption is fitted by a Victoreen expression which is extrapolated beyond the edge. The atomic absorption coefficient is approximated by a second-degree polynomial expression and the remaining long-wavelength oscillations are removed by a multi-iteration curve smoothing, the effect of which is carefully checked. The Haning window applied to the $k^3\chi(k)$ weighted data before Fourier transforming extends from 40 to 700 eV for yttrium and from 45 to 500 eV for zirconium.

The backtransformed contribution of each of the various shells has been analyzed through the classicial EXAFS formula, expressed with the notation

$$\chi(E) = -\sum_j \frac{N_j}{kR_j^2} e^{-2\sigma_j^2 k2} \times e^{-\Gamma_j R_j/k} |f_j(\pi)| \sin(2kR_j + \phi_j)$$

with

$$\phi_j = 2\delta + \psi_j(k),$$

TABLE I

COMPOSITIONS AND PHASE IDENTIFICATION OF THE SAMPLES

Composition	Unit cell symmetry	Crystallographic parameter (M–O distances (Å)) × number	Crystallographic parameter (M–M distances (Å)) × number	Reference
(F) ZrO_2	Monoclinic	(2.051, 2.057, 2.151, 2.163, 2.189, 2.2218, 2.285) × 1 Mean value = 2.16 ± 0.10	(3.341) × 1, (3.433) × 2 (3.461) × 2, (3.463) × 1 Mean value = 3.43 ± 0.10 (3.927) × 2, (4.030) × 2 (4.540) × 1, (3.588) × 1 Mean value = 4.01 ± 0.50	(*10*)
(E) Zr/Y = 10 $Zr_{0.90}Y_{0.10}O_{1.95}$	Tetragonal	(2.046) × 4, (2.433) × 4	(3.618) × 4, (3.633) × 8	(*4*, *11*)
(D) Zr/Y = 2 $Zr_{0.67}Y_{0.33}O_{1.835}$	Cubic fluorite	(2.243) × 7.34[a]	(3.662) × 12	(*4*)
(C) Zr/Y = 0.75 $Zr_{0.43}Y_{0.57}O_{1.715}$	Cubic fluorite	(2.267) × 6.86[a]	(3.703) × 12	(*4*)
(B) Zr/Y = 0.50 $Zr_{0.33}Y_{0.67}O_{1.665}$	Cubic fluorite + Cubic C type	(2.271) × 8[a]	(3.709) × 12[b]	(*4*)
(A) Y_2O_3	Cubic C type	(2.243, 2.268, 2.288, 2.337) × 1.5 Mean value = 2.28 ± 0.05	(3.516, 3.533) × 3 Mean value = 3.52 ± 0.01 (4.000, 4.015) × 3 Mean value = 4.01 ± 0.01	(*8*)

[a] The mean number of M–O first distance in $Zr_{1-x}Y_xO_{2-x/2}$ is $4(2 - x/2)$.

[b] This distance has only been evaluated for the fluorite-type phase.

where δ, ψ_j, and $|f_j(\pi)|$ are respectively the central atom phase shift and the phase and the amplitude of the backscattering atoms, σ is the Debye–Waller-like factor, and Γ is related to the mean free path of the photoelectron. We used either amplitudes and phase shifts extracted from the EXAFS of a model compound when it was available (Y_2O_3) (*8*) or *ab initio* calculations from Teo and Lee (*9*). The origin of the energies E_0 has been taken at the maximum of the K edge found at 17,033 eV for yttrium in Y_2O_3 and at 17,997 eV for zirconium in ZrO_2.

III. Results

A. Analysis of Y_2O_3 and YSZ Phases at the Yttrium Edge

The X-ray absorption structures up to 700 eV beyond the edge are shown in Fig. 1a for some compositions. The signal is so well resolved for Y_2O_3 that oscillations are observed up to 900 eV. As soon as zirconium is introduced in the yttria structure, the radial distribution function around the cations shows a loss of order demonstrated mainly by the disappearance of the third to fifth shells seen in pure yttria (Fig. 2a). YSZ samples present a broad distribution of the Y–O bond lengths, characteristic of the large disorder which seems to strongly affect this bond even for compositions close to pure yttria. That anionic disorder is accompanied by an important decrease of the Y–(Y or Zr) contribution (second shell in the radial distribution function) around the middle of the binary system (B to D). But when the zirconium percentage becomes dominant the yttrium network stabilizes and gives the intense peak seen in sample E.

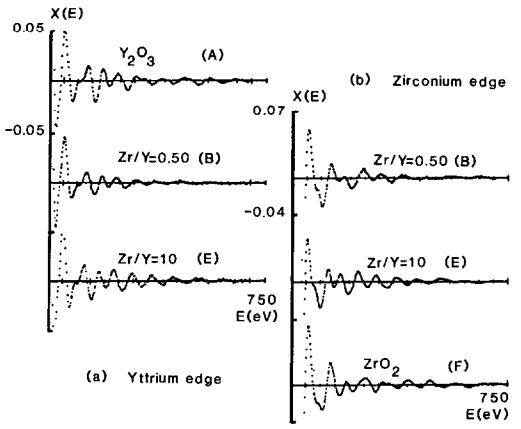

FIG. 1. Experimental spectra of some ZrO_2–Y_2O_3 phases at the (a) yttrium and (b) zirconium K edges.

1. Analysis of the First Oxygen Coordination Shell

Using Teo and Lee backscattering phases and amplitudes, the back Fourier transform of the first oxygen shell of Y_2O_3 is rather well fitted by six atoms at 2.30 Å, a result which agrees with the weighted crystallographic average distance of 2.284 Å (Fig. 3a). This mean value corresponds to three-fourths of the average Y–O distances for Y^{3+} in the C_2 point site added to one-fourth of the average Y–O distance for Y^{3+} in the S_6 point site.

Analysis of samples B, C, D, and E has been performed using experimental amplitudes and phase shifts deduced from Y_2O_3 to fit the Y–O first shell in YSZ phases. The best fits were obtained with the numerical values reported in Table II; Fig. 3b gives an example of the agreement in the case of sample C. The Y–O mean distance remains nearly the same for all the YSZ compounds (2.30 ± 0.02 Å). This value is close to the first Y–O distance in Y_2O_3 and significantly larger than the mean one deduced from an

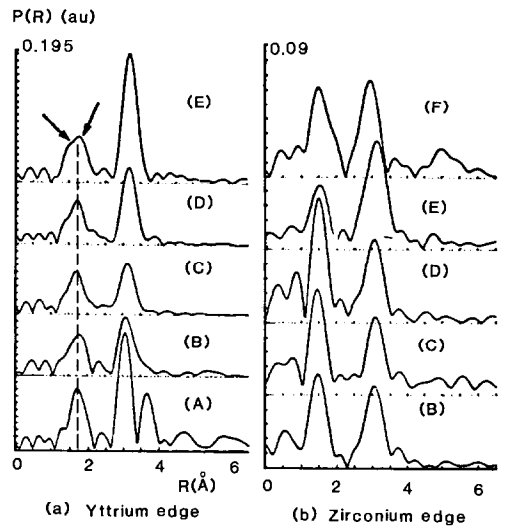

FIG. 2. Modulus of the Fourier transforms of the $k^3\chi(k)$ data at the (a) yttrium and (b) zirconium K edges (uncorrected for phase shifts).

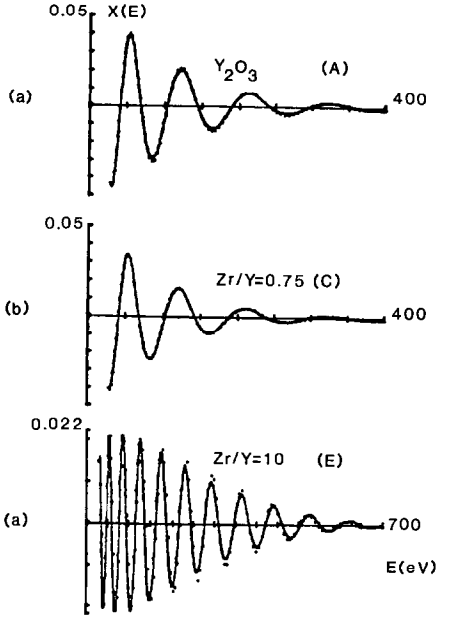

FIG. 3. Some fits between experimental (dots) and calculated (solid lines) signals at the yttrium edge. (a) Y_2O_3 filtered Y–O first shell using Teo and Lee theoretical phases and amplitudes; (b) Zr/Y = 0.75 filtered first shell using corresponding experimental phase and amplitude of Y_2O_3; (c) Zr/Y = 10 filtered second shell using corresponding experimental (Y–Y) phase and amplitude of Y_2O_3.

TABLE II

DISTANCES AND COORDINATION NUMBERS OF THE FIRST COORDINATION SHELL

	Yttrium–oxygen bond			Zirconium–oxygen bond		
Composition	R (Å) ± 0.02	N ± 0.8	$\Delta\sigma$ (Å) ± 0.01	R (Å) ± 0.02	N ± 1.0	$\Delta\sigma$ (Å) ± 0.01
(A) Y_2O_3	2.28	6.0	0.0			
(B) Zr/Y = 0.50	2.28	6.2	0.07	2.14	5.5	0.08
(C) Zr/Y = 0.75	2.29	5.8	0.07	2.17	5.4	0.07
(D) Zr/Y = 2	2.30	6.3	0.07	2.17	7.1	0.08
(E) Zr/Y = 10	2.32	7.5	0.06	2.16		
(F) ZrO_2				2.18	7.9	0.11

ideal fluorite structure (2.27 Å for sample B to 2.24 Å for sample D, see Table I). We have not taken into account the increasing split of this peak from B to E, a split which comes from the continuous increase of the tetragonal phase within the fluorite network. This is particularly obvious in sample E, where the two contributions at 2.05 and 2.43 Å, which stretch apart the 2.28-Å position of the Y–O bond in Y_2O_3, are clearly visible (arrows in Fig. 2a).

The number of oxygen first neighbors remains approximately six for samples B, C, and D as in Y_2O_3 and increases significantly up to 7.5 ± 0.8 for sample E (Zr/Y = 10).

2. Analysis of the Second Metal Coordination Shell

The yttrium second neighbor shell of Y_2O_3 contains two subshells separated by 0.5 Å (Table I), respectively, at the average radius of 3.52 ± 0.01 (six yttrium atoms) and 4.01 ± 0.01 Å (another six yttrium atoms). We attributed the second and third peaks observed in the Fourier transforms to each of these two subshells. We tried to use the amplitudes and phase shifts extracted from the closest subshell to fit the remaining one but did not succeed. The second subshell probably gives rise to large focusing effects due to another oxygen shell which begins at about 4 Å. However, a fourth yttrium shell situated at an average radius of 5.33 Å is rather well fitted using these experimental phase shifts, taking account of the strongly reduced accuracy expected at such a long distance. The third peak due to the C–Ln_2O_3 symmetry disappears in all the YSZ phases, with a small shoulder remaining on the long-distance side of the second peak for sample B, which is situated in the two-phases domain (Table I). The Y–(Y or Zr) peak in YSZ samples has been fitted using amplitudes and phase shifts extracted from Y_2O_3. The similarity of the two elements has not allowed us to separate their contributions. Figure 3c illustrates the agreement between the experimental and calculated filtered back Fourier transforms in the case of sample E. The main features extracted from these fits are:

—A decrease of the number of neighbors in compositions close to the middle of the system (down to 5 for sample C). This is due to a loss of order for the symmetry of the cationic network, a loss which comes from a larger scatter of the corresponding distances (the Debye–Waller factor σ rises by 0.07 Å). When the zirconium content increases, this second subshell is better organized and the number of neighbors goes up to 7.3 for sample E ($\Delta\sigma$ = 0.02 Å).

—A regular increase of the average Y–(Y or Zr) distance: 3.55 (sample B), 3.57 (C), 3.60 (D), and 3.63 Å (E), respectively.

b. Analysis of ZrO_2 and YSZ Phases at the Zirconium Edge

The fine structure curves of B, C, D, and cubic YSZ samples at the Zr edge have a similar shape (Fig. 1b), which is unlike that of phases E (tetragonal) and F (monoclinic pure ZrO_2). Figure 2b gives the Fourier transforms of the $k^3\chi(k)$ data.

For the tetragonal compound the first metal–oxygen peak includes the two M–O distances (about 2.05 and 2.43 Å) expected from the network symmetry. If we consider

only this first cation–oxygen contribution, one can say that the anionic polyhedron is better defined around yttrium than around zirconium, since we separate the two distances better in the case of yttrium (see the split marked by the arrows in Fig. 2a). This point is also supported, by the fact that at the zirconium edge the amplitude of the cation–oxygen contribution is less than for samples D and F, which compositionally border sample E. For the other samples B, C, and D, this first shell becomes well organized and its amplitude is strongly increased as a result of narrowing of the scatter in Zr–O distances. The second shell coming from Zr–(Zr or Y) contributions seems less influenced by the successive yttrium substitutions as compared to the yttrium cation–cation ones described before.

1. Analysis of the First Oxygen Coordination Shell

The structure of monoclinic ZrO_2 described by Smith and Newkirk (*10*) exhibits seven different Zr–O distances ranging from 2.05 to 2.28 Å with an average value of 2.16 ± 0.10 Å. This low symmetry does not allow us to use this oxide as a reference compound so we used theoretical amplitudes and phase shifts to fit the experimental signals.

The results of these fits are given in Table II and Fig. 4a, which show examples of the agreement we obtained between experimental and calculated data in two cases, ZrO_2 (F) and Zr/Y = 0.75 (C). The Zr–O distance for all samples remains close to 2.16 Å as in monoclinic zirconia. The number of oxygen neighbors is evaluated to be eight in sample F and seven in sample D. This number has not been evaluated in E because of the shape of the peak: as we already pointed out, its broadening and the significant decrease of its amplitude compared to B, C, or D reflect the particularly large scattering in the Zr–O distances which occurs in this phase (*11*). In the two compositions (C and B) of lower zirconia content it decreases to about five.

2. Analysis of the Second Metal Coordination Shell

For samples B to D (cubic phases) the Zr–(Zr or Y) bond lengths remain rather unchanged (3.56 to 3.58 Å), therefore slightly more constant than for the yttrium probe (3.55 to 3.60 Å) in the same range of compositions. In sample E (tetragonal sym-

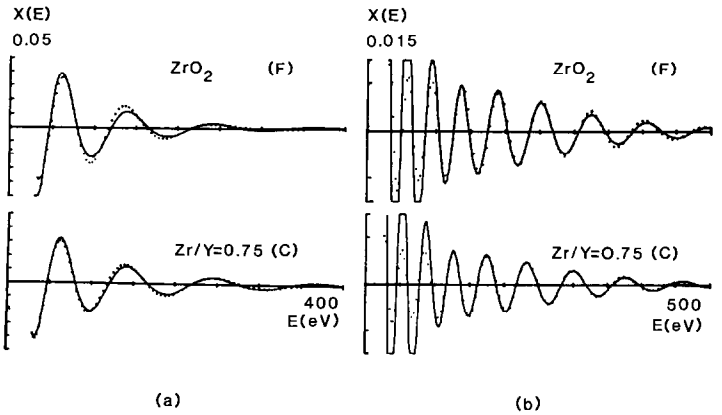

FIG. 4. Examples of fits between experimental (dots) and calculated (solid lines) signals at the zirconium edge using Teo and Lee theoretical phases and amplitudes. (a) Filtered Zr–O first shell of ZrO_2 and Zr/Y = 0.75; (b) filtered second shell (Zr–cation) of ZrO_2 and Zr/Y = 0.75.

metry) this length goes to 3.65 Å (3.63 Å at the yttrium edge). Figure 4b gives examples of the fits obtained in the case of samples C and F.

The number of cation neighbors we found in ZrO_2 (sample F) is six at a mean distance of 3.48 Å, although the X-ray diffraction structural determination (*10*) leads to 12 Zr–Zr distances ranging from 3.43 to 4.03 Å. In fact, the modulus of the Fourier transform is only due to the first six Zr–Zr pairs for which the distances scatter over 0.1 Å around 3.43 Å. The second group of six zirconium neighbors at the average distance of 4.03 Å is displayed over 0.5 Å, so that their respective contributions are cancelled. This is the main difference from Y_2O_3, where the equivalent contribution is clearly visible, the scatter in that case being only 0.01 Å around the mean 4.01-Å Y–Y distance (see Fig. 2a). This is our first evidence to show that the yttrium network is much more destabilized than the zirconium one during the substitutions. This conclusion is also supported by the behavior of the first group of cation–cation amplitudes: their changes are greater when we look at the yttrium probe than when we are at the zirconium edge, where the number of neighbors remains nearly constant whatever the amount of yttrium content (see Fig. 2b).

IV. Discussion and Conclusion

Let us recall the three main points extracted from our analysis of the six compositions examined:

—the structure of the different phases $Zr_{1-x}Y_xO_{2-0.5x}$ is disordered as evidenced by the disappearance of the third to fifth shells, occurring in the pure yttria response;

—the yttrium network appears to be more sensitive to the disorder created by the stabilization process;

—the first Y–oxygen mean distance remains the same (2.30 ± 0.02 Å) for Y_2O_3 and all three cubic YSZ samples as well as in the tetragonal (E) compound. In the same way, the first Zr–oxygen distance keeps the same mean value (2.16 ± 0.02 Å) in ZrO_2 and in all stabilized forms. It appears clear that the oxygen distribution around each cation is characteristic, with the same mean distance as in the corresponding pure oxide: one can notice that the distance calculated for an ideal fluorite structure falls between these two values (see Table I).

The question of the position of oxygen vacancies relative to the cations is of major importance in the structural characterization of stabilized zirconias. The fact that we get only six first neighbors in the immediate surroundings of yttrium for the cubic samples instead of $4(2 - x/2) = 6.7$ for sample B ($\Delta N = 8\%$), 6.9 for C ($\Delta N = 18\%$), and 7.3 for D ($\Delta N = 16\%$), respectively, is consistent with the preferred positions of vacancies as first neighbors of the less charged Y^{3+} ions. This is in accordance with the results already suggested by a previous neutron diffraction investigation (*12*) and, more recently, by low-temperature conductivity measurements (*13*). When the compositions are close to the real YSZ domain, near the ZrO_2 limit, the value we found, 7.5 oxygen atoms for $x = 0.10$ (sample E), is much higher and approaches the theoretical one, 7.8, in this case ($\Delta N = 4\%$). This result agrees with our Eu^{3+} spectroscopic investigation where we found the spectrum characteristic of Eu^{3+} (substituting Y^{3+}) in the six-coordinated C_2 point site in all samples with $x \geqq 0.18$ but not in samples with lower yttria content. Thus it appears that samples with x smaller than about 0.20 differ markedly from those with higher yttria contents and are characterized by a larger number of oxygen neighbors around yttrium. As a matter of fact, in a recent work Catlow *et al.* (*14*) analyzed the EXAFS response of a sample with the $Zr_{0.807}Y_{0.193}O_{1.904}$ composition and concluded that the anion vacancies

are sited adjacent to Zr^{4+} rather than Y^{3+}. The spectroscopic investigation for samples B, C, and D identified environments of 6, 7, and 8 oxygens, whereas EXAFS investigations lead to a mean coordination of six. This number could be slightly higher with lower $\Delta\sigma$ values, less than 0.03. But the agreement we find in sample E (where the coordination number is correct with a $\Delta\sigma$ of 0.06) and the fact that we are adjusting a rather larger scatter of cation–oxygen interatomic distances by a unique average one are in favor of such high $\Delta\sigma$ values. The conclusions are less obvious if we take into account the Zr–O fits since less than six oxygen neighbors are found in samples B and C instead of the eight necessary to attain the stoichiometry. However, as noted in Section III.B.1, the fits at the zirconium edge were done with theoretical phase shifts and amplitudes since we were not able to get a good enough agreement between observed and calculated intensities for the monoclinic ZrO_2 phase, so that we are more confident of numerical values deduced from the yttrium edge signals suggesting the preferential location of two vacancies as first neighbors of yttrium in the B, C, and D cubic samples. The total deficiency of oxygen atom number resulting from the present EXAFS analysis is in fact only questionable for sample C (Table III), in which one can see that the error is about 20%, whereas it is around 10% for B and D, a fairly reasonable difference when using EXAFS to determine the number of neighbors.

Another interesting point is the fits of cation–cation shells for comparison with the mean YSZ structure deduced from X-ray diffraction. The best fits for the Y–cation or Zr–cation shells are obtained with five to six atoms at a mean distance from the central ion which is constant (Zr edge) or slightly increasing (Y edge) from B to D. On the other hand, the cation–cation distances extracted from X-ray diffraction data are larger and decrease from B to D (see Table I). If we consider the ZrO_2 structure, X-ray diffraction measurements take into account the two Zr–Zr subshells, whereas EXAFS only fingerprints the first one because of the strong degree of disorder the zirconium network presents after this first subshell. Within the YSZ phase domain, the second Y or Zr shell is more and more influenced by the loss of order with increasing yttrium content, an increase which in fact corresponds to a higher number of oxygen vacancies from D to B.

TABLE III

TOTAL OXYGEN NUMBER COMPARISON BETWEEN CHEMICAL AND EXAFS ANALYSIS

Composition $Zr_{1-x}Y_xO_{2-0.5x}$	Theoretical oxygen number value $2 - 0.5x$	EXAFS results	Δ (%)
(B) Zr/Y = 0.50 x = 0.67	1.67	1.49	12
(C) Zr/Y = 0.75 x = 0.57	1.72	1.41	22
(D) Zr/Y = 2 x = 0.33	1.84	1.71	8

In conclusion, the present X-ray absorption study brings a complementary insight to the structural characteristics of the so-called yttria-stabilized zirconias by enabling one to distinguish between the two cations. Indeed the anionic neighboring atoms of yttrium are clearly different from those of zirconium, leading to different mean (Y or Zr)–O distances and possibly different mean coordination numbers. These results could not be demonstrated by the other techniques previously used to study this system. The mean Y–cation and Zr–cation distances are the same as in pure oxides within the range of experimental uncertainty, although the yttrium response is qualitatively much more affected by the Zr^{4+}/Y^{3+} substitution than is the zirconium one.

References

1. M. H. TUILIER, J. DEXPERT-GHYS, H. DEXPERT, AND P. LAGARDE, "EXAFS and Near Edge Structure III" (K. O. Hodgson, B. Hedman, and J. E.

Penner-Hahn, Eds.), p. 439, Springer-Verlag, New York/Berlin (1984).
2. A. I. GOLDMAN, E. CANOVA, Y. H. KAO, W. L. ROTH, AND R. WONG, "EXAFS and Near Edge Structure III" (K. O. Hodgson, G. Hedman, and J. E. Penner-Hahn, Eds.), p. 442, Springer-Verlag, New York/Berlin (1984).
3. T. H. ETSELL AND S. N. FLENGAS, *Chem. Rev.* **70,** 339 (1970).
4. J. DEXPERT-GHYS, M. FAUCHER, AND P. CARO, *J. Solid State Chem.* **54,** 179 (1984).
5. V. S. STUBICAN, R. C. HINK, AND S. P. RAY, *J. Amer. Ceram. Soc.* **61,** 17 (1978).
6. C. PASCUAL AND P. DURAN, *J. Amer. Ceram. Soc.* **66,** 23 (1983).
7. J. DEXPERT-GHYS, M. FAUCHER, H. DEXPERT, AND P. CARO, *J. Phys. C* **12,** 7–95 (1977).
8. M. FAUCHER AND J. PANNETIER, *Acta Crystallogr., Sect. B* **36,** 3209 (1980).
9. B. K. TEO AND P. A. LEE, *J. Amer. Chem. Soc.* **101,** 2815 (1979).
10. D. K. SMITH AND H. W. NEWKIRK, *Acta Crystallogr.* **18,** 983 (1965).
11. G. TEUFER, *Acta Crystallogr.* **15,** 1187 (1962).
12. D. STEELE AND B. E. F. FENDER, *J. Phys. C* **7,** 1 (1974).
13. S. P. S. BADWALL, *J. Mater. Sci.* **19,** 1767 (1984).
14. C. R. A. CATLOW, A. V. CHADWICK, G. N. GREAVES, AND L. M. MORONEY, *J. Amer. Ceram. Soc.* **69,** 272 (1986).